

# **Cell – ECM interactions play distinct and essential roles at multiple stages during the development of the aortic arch arteries**

Michael Warkala<sup>1,2</sup>, Dongying Chen<sup>3, §, †</sup>, Ali Jubran<sup>3, §</sup>, AnnJosette Ramirez<sup>1,4, §</sup>, Michael Schonning<sup>1,4, §</sup>, Xia Wang<sup>§, ‡</sup>, and Sophie Astrof<sup>1,2,4\*</sup>.

1. Department of Cell Biology and Molecular Medicine, New Jersey Medical School, Rutgers Biomedical and Health Sciences, Newark, NJ, USA

2. Multidisciplinary Ph.D. Program in Biomedical Sciences: Molecular Biology, Genetics, and Cancer Track, New Jersey Medical School, Rutgers Biomedical and Health Sciences, Newark, NJ, USA

3. Graduate Program in Cell & Developmental Biology, Thomas Jefferson University, Philadelphia, PA, USA

4. Multidisciplinary Ph.D. Program in Biomedical Sciences: Cell Biology, Neuroscience and Physiology Track, New Jersey Medical School, Rutgers Biomedical and Health Sciences, Newark, NJ, USA

† Current address: Yale Cardiovascular Research Center, Department of Internal Medicine, Yale University School of Medicine, New Haven, CT 06511, USA.

‡ Current address: Department of Anatomy, Histology & Developmental Biology, School of Basic Medical Sciences, Shenzhen University Health Science Center, Shenzhen, China

§ These authors contributed equally to the manuscript, and their names are listed in the alphabetical order

Short title: Roles of integrin  $\alpha 5\beta 1$  and fibronectin in aortic arch artery morphogenesis

\* Corresponding author: Sophie Astrof,  
sophie.astrof@rutgers.edu

185 South Orange Ave,  
Medical Sciences Building, Room I-518,  
Newark, NJ, 01703

Total word count:

Subject Codes: Animal Models of Human Disease; Mechanisms; Vascular Biology;

## Abstract

**Rationale:** Defects in the morphogenesis of the aortic arch arteries (AAAs) are among the most severe congenital birth defects. Understanding genes and mechanisms regulating AAA formation and remodeling will provide important insights into the etiology and potential treatments of congenital heart disease.

**Objective:** Cell-ECM interactions play essential roles in the AAA morphogenesis; however, their specific functions are not well-understood. Previously, we demonstrated that integrin  $\alpha 5 \beta 1$  and fibronectin (Fn1) expressed in the Isl1 lineage and its derivatives regulate the formation of the pharyngeal arch arteries (PAAs), the vessels giving rise to the AAAs. The objective of these studies was to investigate the mechanisms by which integrin  $\alpha 5 \beta 1$  and Fn1 regulate AAA morphogenesis.

**Methods and Results:** Using temporal lineage tracing, we found that endothelial progenitors of the AAA endothelium arise early during the development of the second heart field (SHF) and that the 4<sup>th</sup> PAAs contain the highest percentage of the SHF-derived ECs (ECs). To understand the role of cell-extracellular matrix (ECM) interactions in AAA development, we deleted either integrin  $\alpha 5$  or its major extracellular ligand Fn1 in the Isl1 lineage. We used whole-mount confocal imaging to define the complex spatial and temporal EC dynamics during PAA formation at the quantitative level and assessed how cell-ECM interactions modulated these dynamics. Our analyses demonstrated that integrin  $\alpha 5 \beta 1$  and Fn1 mediate AAA morphogenesis by regulating the accrual of SHF-derived endothelium into the 4<sup>th</sup> pharyngeal arches and the remodeling of the 4<sup>th</sup> pharyngeal arch EC plexus into the PAAs. Following PAA formation, integrin  $\alpha 5 \beta 1$  is essential for the activation of Notch in the neural crest-derived cells surrounding the 4<sup>th</sup> PAAs and for the differentiation of the neural crest cells into vascular smooth muscle cells.

**Conclusions:** Our data demonstrate that cell-ECM interactions regulated by integrin  $\alpha 5 \beta 1$  and Fn1 function reiteratively during AAA development to mediate the multi-step process of AAA morphogenesis.

Key Words: integrin  $\alpha 5\beta 1$ , second heart field, endothelial progenitor cells, pharyngeal arch arteries, aortic arch arteries

**Nonstandard Abbreviations and Acronyms in the Alphabetical Order:** AAA – aortic arch arteries, AHF – anterior heart field, CHD – congenital heart disease, ECs – endothelial cells, IAA-B – interrupted aortic arch type B, PAA – pharyngeal arch arteries, RERSA – retro-esophageal right subclavian artery, SHF – second heart field, VEGFR2 – Vascular endothelial growth factor receptor 2,

## Introduction

Aortic arch arteries (AAAs) comprise an asymmetrical vascular tree that routes oxygenated blood from the heart into the systemic circulation (Stoller and Epstein, 2005). Defects in the development of the AAAs cause devastating forms of congenital heart disease (CHD) due to interruption(s) in the aortic arch and often occur in conjunction with the 22q11 deletion syndromes (Scambler, 2000). Cumulatively, four prospective studies found that 40 – 90% cases of the interrupted aortic arch in fetuses, neonates, and children can be attributed to deletions in the 22q11 region (Momma, 2010). Non-lethal defects in AAA morphogenesis can cause discomfort and affect the quality of life due to vascular rings restricting eating and breathing, or due to dizziness, vertigo, and tinnitus (Psillas et al., 2007). Significantly, studies using *Tbx1*<sup>+/-</sup> mice that model 22q11  $\Delta$  syndrome indicated that defective formation of the left 4<sup>th</sup> PAA underlies IAA-B. Intriguingly, several labs demonstrated that *Tbx1* regulates the expression of integrins and extracellular matrix (ECM) components, and showed that defects in cell-ECM interactions precede pathological sequelae and cardiovascular defects in *Tbx1* mutants. (Alfano et al., 2019; Francou et al., 2014). However, mechanisms by which signaling by ECM regulates PAA formation are not well-understood. Thus, investigating the roles of cell-ECM interactions in PAA morphogenesis will provide novel insights into the mechanisms of PAA formation and will improve the knowledge of how alterations in cell-ECM interactions result in IAA-B.

The AAAs develop from three bilaterally symmetrical pairs of pharyngeal arch arteries (PAA), numbered 3, 4, and 6, that undergo stereotypical steps of asymmetrical regression and remodeling (Kirby, 2007). Thus, phenotypically identical AAA defects can arise due to either of the two distinct mechanisms: 1) defects in PAA formation or 2) defects in the remodeling of symmetric PAAs into asymmetric AAAs (Moon, 2008). PAAs arise by vasculogenesis from endothelial precursors originating in the lateral plate mesoderm, also known as the second heart field (Abrial et al., 2017; Bremer, 1912; DeRuiter et al., 1993; Li et al., 2012; Nagelberg et al., 2015; Paffett-Lugassy et al., 2013; Wang et al., 2017). Experiments in zebrafish and mice demonstrated that PAA formation is a multi-stage process that entails endothelial specification in the SHF,

migration of SHF-derived endothelial progenitors into the pharyngeal region, differentiation into ECs, and the assembly of SHF-derived ECs into a plexus of small blood vessels (Abrial et al., 2017; Guner-Ataman et al., 2018; Guner-Ataman et al., 2013; Holowiecki et al., 2020; Wang et al., 2017). Thereafter, the pharyngeal endothelial plexus becomes connected with the ventral and dorsal aortae. The endothelium of the ventral aortae forms by vasculogenesis from SHF-derived progenitors and is contiguous with the cardiac outflow tract (Bremer, 1912; Wang et al., 2017). Following pharyngeal arch segmentation, plexus endothelium in pharyngeal arches rearranges by the coalescence of uniform, small blood vessels into one large arterial blood vessel in each pharyngeal arch, connecting the outflow tract of the heart via the ventral aortae with the dorsal aortae (Wang et al., 2017). The 3<sup>rd</sup> PAA is evident by E9.5, before the formation of the 4<sup>th</sup> and 6<sup>th</sup> PAAs. By the evening of E10.5, the three symmetrical pairs of PAAs are fully formed. Following PAA formation, neural crest-derived cells closest to the PAA endothelium differentiate into vascular smooth muscle cells (VSMCs), and nearly fully surround the PAA endothelium with the VSMC coat by E12.5 (Bockman et al., 1987; Gittenberger-de Groot et al., 1999; Hutson and Kirby, 2007; Hutson et al., 2009; Rosenquist et al., 1989). The differentiation of neural crest (NC)-derived cells into VSMCs is essential for the stability of the PAAs, and for their eventual remodeling into the asymmetrical AAAs; Defects in NC differentiation lead to arch artery regression and CHD (Hutson and Kirby, 2007; Hutson et al., 2009; Keyte and Hutson, 2012).

Previously, we demonstrated that the expression of integrin  $\alpha 5\beta 1$  or fibronectin (Fn1) in the Isl1 lineages was required for the formation of the 4<sup>th</sup> PAA (Chen et al., 2015). To understand the mechanisms by which integrin  $\alpha 5\beta 1$  and Fn1 regulate AAA development, we analyzed EC dynamics during PAA formation and remodeling from E9.5 until E11.5 of embryonic development, representing the crucial stages in AAA morphogenesis. Our studies point to the essential roles of integrin  $\alpha 5\beta 1$  and cell-ECM interactions at multiple stages of PAA biogenesis and remodeling.

## Methods

**Animals** C57BL/6J mice (cat # 0664) were purchased from Jackson Laboratories. Integrin  $\alpha 5^{+/-}$  and integrin  $\alpha 5^{flox/flox}$  mice were gifts from Dr. Richard Hynes (van der Flier et al., 2010; Yang and Hynes, 1996).  $Isl1^{Cre}$  and  $Isl1^{CreER}$  knock-in mice were gifts from Dr. Sylvia Evans (Cai et al., 2003; Sun et al., 2007), MEF2C-AHF-DreERT2 transgenic mice were a gift from Dr. Benoit Bruneau (Devine et al., 2014),  $Sox17^{2A-iCre}$  knock-in mice were a gift from Heicko Lickert (Engert et al., 2009),  $Rosa^{mTmG}$  mice,  $Gt(ROSA)26Sortm4(ACTB-tdTomato,-EGFP)$  (Muzumdar et al., 2007) and B6;129S6- $Gt(ROSA)26Sor^{tm1(CAG-tdTomato*, -EGFP*)Ees/J}$ , known as  $ROSA^{nT-nG}$  mice, generated by Justin Prigge and Ed Schmidt at Montana State University, were purchased from Jackson labs; In this strain, two distinct nuclear localization signals derived from human SRm160 protein (Wagner et al., 2003) were fused with tdTomato and EGFP sequences. Dre reporter mice were a gift from Dr. Hongkui Zeng (Madisen et al., 2015). Mice and embryos were genotyped according to published protocols. Mice were housed in an AAALAC-approved barrier facility. All experimental procedures were approved by the Institutional Animal Care and Use Committee of Rutgers University and conducted in accordance with the Federal guidelines for the humane care of animals.

**Tamoxifen injections** Tamoxifen was dissolved either in corn oil or in sesame oil at the concentration of 10 mg/ml. Labeling was done by injection 300  $\mu$ l of this stock into pregnant females at E7.5, E8.5, or E9.5, at the time points specified in figure legends. Embryos were dissected at E10.5, staged by counting somites, stained, and imaged by using confocal microscopy, and quantifications were performed as described in (Ramirez and Astrof, 2020)..

**Whole Mount Immunofluorescence staining** Embryos were isolated at specified days of development, fixed in 4% paraformaldehyde (PFA) at 4°C overnight, rinsed in PBS and either used immediately, or dehydrated through a series of 25%, 50%, and 75% of methanol dilutions in PBS, then washed with three times with 100% methanol and stored in 100% methanol at -20°C until use. The following antibodies were used 1° antibodies: anti-Pecam1 (1:200, BD Pharmingen, cat #550274), anti-VEGFR2 (1:200, R&D, cat #AF644), anti-ERG (1:1000, Abcam, cat# ab214341), anti-GFP (1:300, Aves,

cat #GFP1020), 2° antibodies were from Invitrogen and used at the dilution of 1:300. Nuclei were stained using DAPI (1:1000 dilution of 5 mg/ml stock made in H<sub>2</sub>O, Sigma, cat #32670-5MG-F). Following washes, stained embryos were embedded into 1% agarose (Bio-Rad Laboratories, cat #1613101), cleared using Benzyl Alcohol (Sigma, cat # B-1042)/ Benzyl Benzoate (Sigma, cat #B-6630), placed between two #1.5 coverslips (VWR, cat #16004-312) separated by a rubber spacer (Grace Bio Labs, cat # 664113). Confocal imaging was done using Nikon A1R microscopes with 20x CFI Apo LWD Lambda S water immersion objective (MRD77200) or 25x CFI Plan Apo Lambda S silicone oil objectives (MRD73250). Images were analyzed, and endothelial populations were quantified using IMARIS software (Bitplane, USA) (Wang et al., 2017) and (Ramirez and Astrof, 2020).

## Results

### SHF contributes to PAA endothelium during a short developmental window

Previous work from our lab demonstrated that in the mouse, the majority of PAA endothelium is derived from the SHF, labeled by either Mef2C-AHF-Cre- or Isl1-expressing mesodermal lineages. (Wang et al., 2017). To analyze the contribution of the SHF to the PAA endothelium at a quantitative level, we imaged the entire pharyngeal arch regions corresponding with the arches 3, 4, and 6, and quantified the proportion of SHF-lineage labeled ECs in the PAAs (Fig. 1). Our analyses demonstrated that although each PAA contains a similar number of ECs (Fig. 1B), the 4<sup>th</sup> PAA endothelium contains the highest proportion of SHF-derived cells (Fig 1C – C'), while the endothelium of the 3<sup>rd</sup> PAA contains the lowest contribution from the SHF (Fig. 1C – C'). These observations suggest that genes affecting the development of SHF-derived ECs may have the highest impact on the morphogenesis of the 4<sup>th</sup> PAAs and their derivatives.

To define the temporal window during which the SHF mesoderm harbors progenitors of the PAA endothelium, we used *Isl1*<sup>CreER</sup> knock-in mice (Sun et al., 2007) and Mef2C-AHF-DreERT2 transgenic mice (Devine et al., 2014) together with discrete pulses of

tamoxifen to lineage-label the SHF mesoderm at different developmental times (Fig. 2). Tamoxifen was injected at discrete time points at E6.5 – E9.5, embryos were dissected at E10.5, stained to detect lineage labeling in the PAA endothelium. Entire pharyngeal regions were imaged using confocal microscopy to quantify the contribution of lineage-labeled cells to the PAA endothelium. The peak labeling in the PAAs occurred when tamoxifen was injected at 5 AM at E7.5 in *Isl1<sup>CreER</sup>* strain (Fig. 2A) and 10 PM at E7.5 in Mef2C-AHF-DreERT2 strain (Fig. 2B). While tamoxifen injection into *Isl1<sup>CreER</sup>* resulted in sparse labeling of PAA ECs, the injection of tamoxifen into Mef2C-AHF-DreERT2 transgenic mice led to the labeling of a much larger proportion of ECs in the PAAs (Fig. 2B). These differences likely reflect that: 1) CreER is a knocked into the *Isl1* locus generating an *Isl1-null* allele, e.g. *Isl1<sup>CreER</sup> / +* mice are *Isl1<sup>+/-</sup>* (Sun et al., 2007), while Mef2C-AHF-DreERT2 is a transgenic strain containing multiple copies of the Mef2C-AHF-DreERT2 transgene (Devine et al., 2014); 2) the expression of *Isl1* is downregulated commensurate with endothelial differentiation (Jia et al., 2018); thus potentially low levels of CreER expression in *Isl1<sup>CreER</sup>* mice could have resulted in low labeling of endothelial progenitors relative to that of Mef2C-AHF-DreERT2 strain. The cardiac labeling using *Isl1<sup>CreER</sup> / +* mice at all stages tested was extensive, as described (Sun et al., 2007), indicating that our labeling technique was consistent with previous studies (data not shown). The difference in the timing of peak endothelial labeling in the PAAs between *Isl1<sup>CreER</sup>* and Mef2C-AHF-DreERT2 strains is likely due to the earlier onset of *Isl1* expression compared with the expression of the MEF2C-AHF-Cre transgene; In fact, *Isl1* regulates the expression of Mef2C and the activation of the Mef2C-AHF enhancer (Dodou et al., 2004; Verzi et al., 2005); Correspondingly, our experiments demonstrate that the peak endothelial labeling of PAAs in *Isl1<sup>CreER</sup>* strain precedes that of Mef2C-Dre-ERT2 strain by 17 hours (Fig. 2A, B). These studies indicate that the SHF mesoderm harbors PAA endothelial progenitors for the 3<sup>rd</sup> PAA between E7.5 and E8.5 of embryonic development and the 4<sup>th</sup> and 6<sup>th</sup> PAAs, between E7.5 and E9.5 (Fig. 2B, 2B1, 2B2). In summary, these data show that the 4<sup>th</sup> PAAs differ from the 3<sup>rd</sup> and the 6<sup>th</sup> PAAs in the proportion of SHF-derived cells. In addition, the 4<sup>th</sup> and 6<sup>th</sup> PAAs differ from the 3<sup>rd</sup> PAA in the timing during which SHF cells are added.

## **Integrin $\alpha 5\beta 1$ is not required for the migration of SHF-derived cells into the heart and the pharyngeal arches, or the maturation of SHF-derived ECs**

Our previous studies demonstrated that the expression of integrin  $\alpha 5\beta 1$  or Fn1 in the Isl1 lineages is required for the formation of the 4<sup>th</sup> PAAs (Chen et al., 2015). We showed that these deletions resulted in the Interrupted Aortic Arch Type B (IAA-B) and retro-esophageal right subclavian artery (RERSA), consistent with the defective development of the 4<sup>th</sup> PAAs observed at E10.5 in these mutants (Chen et al., 2015). To determine mechanisms by which integrin  $\alpha 5\beta 1$  and Fn1 regulate PAA development, we analyzed PAA formation at three distinct stages of development using whole-mount immunofluorescence followed by quantitative analyses of SHF-derived populations and endothelial dynamics.

We began our analysis at E9.5, before the time when the segmentation of the pharyngeal arches is complete. At this time of development, the PAA endothelium exists as a plexus of ECs expressing vascular endothelial growth factor receptor 2 (VEGFR2) in the pharyngeal mesenchyme (Li et al., 2012). To quantify the number of SHF-derived cells, including SHF-derived VEGFR2<sup>+</sup> cells in the pharyngeal arches, we used ROSA<sup>nT-nG</sup> reporter mice, in which nuclear localization sequences are fused with tdTomato and EGFP sequences, leading to the expression and nuclear localization of EGFP upon Cre-induced recombination. We quantified the number of SHF-derived cells in the heart and the pharyngeal region but did not see differences between controls and mutants (Fig. 3A-D). The differentiation of SHF-lineage cells (GFP<sup>+</sup>) into VEGFR2<sup>+</sup> cells within the pharyngeal mesenchyme was not altered either (Fig. 3E). We also did not see differences in the maturation of VEGFR2<sup>+</sup> cells into Pecam1<sup>+</sup> cells between controls and mutants at E10.5 (Sup. Fig. 1).

## **Integrin $\alpha 5\beta 1$ and fibronectin regulate the accrual of SHF-derived ECs into the 4<sup>th</sup> pharyngeal arches between E9.5 and E10.5**

We found that mutants with defective 4<sup>th</sup> PAAs contained fewer ECs in the 4<sup>th</sup> pharyngeal arches at 32 – 33 somites at about 2 PM of E10.5 (Fig. 4A, Sup. Fig. 2A-D). Despite this decrease in EC numbers, the size of the 4<sup>th</sup> arches, the tissues within which

PAA formation, was not affected (Fig. 4B). Since the pharyngeal mesenchyme is mainly composed of neural crest cells, these findings indicate that neural crest recruitment and pharyngeal arch formation proceed normally in the mutants. Interestingly, the number of ECs in the mutants recovered by about 6 PM of E10.5 and was similar to that of controls (Fig. 4C); by this time, embryos reached the 36 – 39 somite stage. Our quantitative analyses indicate that PAA formation phenotypes in integrin  $\alpha 5^{f/-}; Isl1^{Cre/+}$  and  $Fn1^{f/-}; Isl1^{Cre/+}$  mutants are indistinguishable from one another (Sup. Fig. 2B – E), and therefore, we will refer to integrin  $\alpha 5^{f/-}; Isl1^{Cre/+}$  and  $Fn1^{f/-}; Isl1^{Cre/+}$  embryos collectively, as mutants. These studies indicate that there is a temporary dip in the accumulation of endothelial cells in the 4<sup>th</sup> pharyngeal arches.

### **Integrin $\alpha 5\beta 1$ and fibronectin regulate the remodeling of pharyngeal plexus into the PAA independent of endothelial cell numbers.**

The formation of the 4<sup>th</sup> PAAs can be followed at different time points during the 10<sup>th</sup> day of embryonic mouse development. In controls, plexus ECs in the 4<sup>th</sup> arch begin coalescing into the PAA when embryos are between 30 and 32 somites (Wang et al., 2017) (Sup. Fig. 3). These rearrangements result in an initially thin PAA, in which approximately 50% of the pharyngeal arch ECs are redistributed into the PAA by 32 -34 somite stage (Wang et al., 2017). As the development proceeds, close to 60% of the 4<sup>th</sup> pharyngeal arch endothelium is redistributed into the PAA by the evening of E10.5 (Wang et al., 2017). Thus, the percentage of pharyngeal arch endothelium in the PAA can be taken as a measure of PAA formation.

Despite the recovery of EC numbers by the evening of E10.5, PAAs looked thin in the affected mutants (Fig. 5A-L and Sup. Fig. 2A), and the proportion of ECs in the 4<sup>th</sup> PAAs was nearly 2-fold lower in the mutants compared with controls (Sup. Fig. 2E), indicating a defect in the rearrangement of the plexus endothelium into the PAA. To further understand the mechanisms by which integrin  $\alpha 5$  and Fn1 regulate PAA formation, we examined EC dynamics in control and mutant embryos at three-time points, corresponding with 32 – 33 somites, 34 – 35 somites, and 36 – 39 somites. These stages span about 6 hours of development from 12 PM to 6 PM on the 10<sup>th</sup> day of

mouse embryonic development. The formation of the 4<sup>th</sup> PAAs lagged both in integrin  $\alpha 5^{f/-}$ ;  $Isl1^{Cre/+}$  and  $Fn1^{f/-}$ ;  $Isl1^{Cre/+}$  mutants at all time points tested during E10.5 (Fig. 5M and Sup Fig. 2E), and in 7 of 16 of these, the 4<sup>th</sup> PAAs were absent at 32 – 34 somite stage (Fig. 5A-F, and Sup. Fig. 2E), a stage in which close to 50% of the endothelium in controls is located in the 4<sup>th</sup> PAAs (Wang et al., 2017) (Fig. 5M). This difference in the distribution of ECs between the PAA and the plexus did not result from defective proliferation or survival of ECs (Fig. 5N). BrdU incorporation into the endothelium of the 4<sup>th</sup> PAA and plexus was comparable between controls and mutants Fig. 5N). Similar to controls, BrdU incorporation into the plexus endothelium was 2-fold higher than that into the PAA in the mutants. These data indicate that proper rearrangement of endothelial plexus is required for the normal morphogenesis of the AAAs.

Since mutant embryos had fewer ECs in the 4<sup>th</sup> pharyngeal arches compared with controls prior to the 36<sup>th</sup> somite stage, we performed correlation analyses to determine whether the formation of the 4<sup>th</sup> PAAs depended on EC numbers or EC density in the 4<sup>th</sup> pharyngeal arches. As described above, the percentage of pharyngeal arch endothelium in the PAA relative to the plexus can be taken as a measure of PAA formation (Wang et al., 2017). For these analyses, we quantified EC numbers in control embryos isolated between 32 to 39 somite stages. Despite the sharp increase in the number of ECs in the 4<sup>th</sup> arches between these stages (Wang et al., 2017), the formation of the 4<sup>th</sup> PAAs was not dependent on the EC number or EC density in controls (Fig. 6A-B). Similarly, correlation analysis of PAA formation in the mutants with defective and normal 4<sup>th</sup> PAAs, showed that just like in controls, the rearrangement of plexus ECs into the PAA did not depend on the number of ECs in the mutants (Fig. 6C). Next, we compared PAA formation in controls and mutants that had similar numbers of ECs in the 4<sup>th</sup> arches (Fig. 6D). These analyses showed that in groups of mutant and control embryos with similar numbers of ECs, the percent of ECs in PAAs was lower in the mutants Fig. 6D). Together, these data indicate that the reorganization of plexus ECs into the PAA in the 4<sup>th</sup> arch does not depend on the EC number. Taken together, these studies indicate that during the 10<sup>th</sup> day of embryonic development, cell – ECM interactions mediated by integrin  $\alpha 5\beta 1$  and  $Fn1$  are essential for the remodeling of the initially uniform vascular plexus into the PAA in the 4<sup>th</sup> pharyngeal arches.

## **The expression of integrin $\alpha 5$ in the *Isl1* lineage is required for the differentiation of neural crest cells into vascular smooth muscle cells.**

To determine whether the rearrangement of the endothelial plexus in the 4<sup>th</sup> arch was blocked or delayed, we examined E11.5 embryos, expecting to find absent or diminished 4<sup>th</sup> PAAs in the mutants. However, contrary to our expectations, the formation of the 4<sup>th</sup> pharyngeal arch arteries has recovered in the mutants by this time, and the perimeters of PAA vessel cross-sections in the mutants were comparable to those of controls (Fig. 7A, n=8). Since 50% of *integrin  $\alpha 5^{flox/-}; Isl1^{Cre}$*  mutants develop 4<sup>th</sup> arch artery defects, such as IAA-B and RERSA (Chen et al., 2015), these data indicated that the 4<sup>th</sup> PAAs eventually regress in the mutants. Arch artery regression is most commonly caused by the defective differentiation of neural crest cells surrounding the arch artery endothelium into vascular smooth muscle cells, VSMCs (Hellstrom et al., 2001; High et al., 2009; High et al., 2008; High et al., 2007; Manderfield et al., 2015; Manderfield et al., 2012). To determine whether this process was affected in the mutants, we analyzed VSMC differentiation in the pharyngeal arches. For these experiments, we calculated the fraction of vessel perimeter covered by smooth muscle actin (SMA)-expressing cells, using the methodology we developed previously (Wang and Astrof, 2016). We found that the differentiation of neural crest cells into VSMCs was severely diminished around PAAs in the mutants (Fig. 8B). The decrease in  $\alpha$ SMA expression was not due to neural crest cell death (Sup. Fig. 4). Since the *Isl1* lineage marks some neural crest cells (Engleka et al., 2012), we tested whether the *Isl1* lineage marker marked the neural crest cells surrounding the PAAs. However, this was not the case (Fig. 7C), indicating that integrin  $\alpha 5$  regulates neural crest differentiation non-cell-autonomously. These results are consistent with our previous experiments demonstrating that the expression of integrin  $\alpha 5$  in the *Mesp1* lineage marking the anterior mesoderm regulates the differentiation of neural crest cells into VSMCs around the 4<sup>th</sup> PAA (Liang et al., 2014), and suggest that the expression of integrin  $\alpha 5$  in the *Isl1* lineage, most likely in the second heart field mesoderm, regulates neural crest differentiation. Since the deletion of integrin  $\alpha 5$  in the *Mesp1* lineage does not result in defective or delayed PAA formation (Liang et al., 2014), our studies also indicate that

integrin  $\alpha 5$  expressed in the *Isl1* lineage plays an independent, and a later role in arch artery morphogenesis, namely in the differentiation of neural crest-derived cells into VSMCs. Furthermore, these data indicate the defect in VSMC differentiation in *integrin  $\alpha 5^{flox/-}; Isl1^{Cre}$*  mutants is not merely due to the delayed accrual of arch artery endothelium, or delayed remodeling of the vascular plexus in the 4<sup>th</sup> pharyngeal arch into the PAA.

The differentiation of neural crest cells into VSMCs is orchestrated in part by a relay of Notch signaling transduced from the arch artery endothelium to the surrounding layers of neural crest cells. The activation of Notch signaling in the neural crest is required for the differentiation of neural crest cells into VSMCs (High et al., 2007; Manderfield et al., 2012). We demonstrated that this pathway was regulated by the expression of integrin  $\alpha 5$  and fibronectin in neural crest cells (Wang and Astrof, 2016). To test the possibility that the expression of integrin  $\alpha 5$  in the *Isl1* lineages regulates the lateral propagation of Notch signaling from the PAA endothelium to the neural crest-derived cells, we stained sections with an antibody to Notch Intracellular Domain (NICD), an activated form of Notch. However, Notch signaling was activated comparably in controls and mutants, despite the severe deficiency in the differentiation of neural crest cells into VSMCs in the mutants (Fig. 7C). These experiments indicate that the expression of integrin  $\alpha 5$  in the pharyngeal arch mesoderm regulates the differentiation of neural crest cells into VSMCs independently of Notch. Furthermore, these experiments indicate that while the activation of Notch is necessary for the differentiation of neural crest cells into VSMCs, it is not sufficient. Taken together, the studies in this manuscript demonstrate that cell-ECM interactions regulated by integrin  $\alpha 5$  play multiple, pleiotropic, and stage-specific functions during the morphogenesis of the 4<sup>th</sup> PAAs.

### **Multiple lineages in the pharynx require the concomitant expression of integrin $\alpha 5$ and fibronectin to regulate the formation of the 4<sup>th</sup> PAAs.**

The *Isl1* lineages encompass mesoderm of the SHF, pharyngeal endoderm, surface ectoderm, and some neural crest cell populations (Engleka et al., 2012; Sun et al., 2007). Our previous studies indicated that the expression of integrin  $\alpha 5$  or Fn1 in the

surface ectoderm and the neural crest was not required for the formation of the 4<sup>th</sup> PAA (Chen et al., 2015; Wang and Astrof, 2016). The deletion of either integrin  $\alpha 5$  or Fn1 in the SHF lineage using the Mef2C-AHF-Cre transgenic line resulted in live progeny at the correct Mendelian ratios (Sup. Tables 1 and 2), indicating that the expression of integrin  $\alpha 5$  or Fn1 in the SHF alone is not required for cardiovascular development. Consistent with these findings, the expression of integrin  $\alpha 5$  in the *Mesp1* lineage or in the endothelium was also not required for PAA formation (Liang et al., 2014; van der Flier et al., 2010). Lastly, to test whether the expression of integrin  $\alpha 5$  in the endoderm regulated PAA formation, we used the constitutive Sox17<sup>2A-iCre</sup> knockin line, in which Cre is expressed in the endoderm and some endothelia (Engert et al., 2009). However, PAAs formed normally in  $\alpha 5^{fllox/-}; Sox17^{2A-iCre}$  mutants (Sup. Fig. 5). Together, these data indicate that combinatorial expression of integrin  $\alpha 5$  and Fn1 in the Isl1 lineages is necessary for the proper formation of the 4<sup>th</sup> PAAs.

## Discussion

Proper development of the 4<sup>th</sup> PAAs is central to the ability of a newborn to survive and thrive (Karunamuni et al., 2014; Moon, 2008). The formation of the 4<sup>th</sup> pair of the PAAs is regulated by a number of genes including *Tbx1*, *Pax9*, *Gbx2*, *Fgf8*, *Crkl*, *PlexinD1*, and *Nrp1*, e.g., (Calmont et al., 2009; Gitler et al., 2004; Macatee et al., 2003; Merscher et al., 2001; Phillips et al., 2019). However, particular aspects of PAA formation regulated by these genes are not well-understood. Unraveling EC dynamics by which PAAs form is vital to understanding the processes regulated by disease genes in congenital heart disease.

In this manuscript, we have demonstrated that endothelial progenitors of the PAA endothelium are present early during the ontogeny of the SHF and that the SHF is the primary source of the PAA endothelium. Furthermore, we showed that the 4<sup>th</sup> PAA contains the largest proportion of SHF-derived cells compared with the 3<sup>rd</sup> and the 6<sup>th</sup> PAA pairs. These studies suggest that mutations affecting the development of the SHF would affect the 4<sup>th</sup> PAAs more profoundly than the 3<sup>rd</sup> and the 6<sup>th</sup> PAAs.

By using whole-mount imaging and quantitative analyses of EC populations in the pharyngeal arches, we previously demonstrated that the morphogenesis of the 4<sup>th</sup> PAAs occurs gradually throughout the 10<sup>th</sup> day of the embryonic development and entails a rapid accrual of ECs: an endothelial population more than triples in about eight hours of development, from 30 – 39 somites, taking place between 10 am and 6 pm of the same day (Wang et al., 2017). This steep increase is unlikely to occur solely due to EC proliferation, and our labeling experiments show that SHF-derived cells still harbor EC progenitors that are being added to the 4<sup>th</sup> PAA after E8.5. EC population in the 4<sup>th</sup> arch of the mutants temporarily dips between E9.5 and E10.5, suggesting that integrin  $\alpha 5$  and Fn1 are important for this later accrual of SHF-derived ECs to the 4<sup>th</sup> arch.

A uniform vascular plexus present in the 4<sup>th</sup> arch on the morning of E10.5 begins rearranging by the coalescence of ECs into the PAA, and by about noon of the tenth day of development, when embryos reach 32 – 34 somites, about 50% of arch ECs in the 4<sup>th</sup> arch have coalesced to form a thin PAA (Wang et al., 2017). At this time, small blood vessels of the plexus are connected with the expanding PAA, and as the coalescence proceeds, the spaces between the PAA and the plexus vessels disappear, and eventually, by 36 – 39 somites, the majority of the 4<sup>th</sup> arch ECs are located within the PAA (Wang et al., 2017) and (Sup. Fig. 3). Despite the initial deficiency of EC numbers in the 4<sup>th</sup> arch, endothelial population recovers in integrin  $\alpha 5^{f/-}$ ; *Isl1<sup>Cre/+</sup>* and *Fn1<sup>f/-</sup>*; *Isl1<sup>Cre/+</sup>* mutants by the 34 – 35 somite stage; however, in spite of this recovery, the 4<sup>th</sup> PAAs were either thin or absent in 50% of all the 4<sup>th</sup> arches examined (Fig. 5 and Sup. Fig. 2) (Chen et al., 2015). Interestingly, our regression analysis showed that the rearrangement of the 4<sup>th</sup> pharyngeal arch endothelium into the PAA was not dependent on the number or density of ECs in the 4<sup>th</sup> arch in embryos ranging from 32 – 29 somites. These data suggest that the regulation of plexus-to-PAA remodeling in the 4<sup>th</sup> arch is mediated by factors extrinsic to the PAA endothelium, and the disruption of the remodeling in the mutants indicates an essential role for cell – ECM in this process.

The PAAs form within the neural crest-derived pharyngeal mesenchyme and the PAA endothelium induces the differentiation of the adjacent neural crest-derived cells into VSMCs. Despite the initial delay in the formation of the 4<sup>th</sup> PAAs, the size of PAAs in

integrin  $\alpha 5^{f/-}$ ;  $Isl1^{Cre/+}$  mutants recovered by E11.5. At this time, we observed a profound deficiency in the expression of  $\alpha$ SMA in the surrounding neural crest-derived cells around the left PAAs in the mutants. This defect is consistent with our findings that about 50% of integrin  $\alpha 5^{f/-}$ ;  $Isl1^{Cre/+}$  and  $Fn1^{f/-}$ ;  $Isl1^{Cre/+}$  mutants develop lethal AAA defects in late gestation (Chen et al., 2015). While we cannot rule out that the delay in the formation of the 4<sup>th</sup> PAA led to the deficient differentiation of smooth muscle cells in our mutants, our previous studies using integrin  $\alpha 5^{f/-}$ ;  $Mesp1^{Cre/+}$  mice demonstrated that the expression of integrin  $\alpha 5$  in the mesoderm regulates neural crest differentiation into VSMCs without affecting PAA formation (Liang et al., 2014). Thus, the roles of integrin  $\alpha 5$  and  $Fn1$  in the formation of the 4<sup>th</sup> PAA are separate from their roles in the differentiation of the neural crest cells into VSCMs (Wang and Astrof, 2016). Taken together, our studies indicate that cell-ECM interactions regulated by integrin  $\alpha 5$  and  $Fn1$  play pleiotropic and indispensable roles at multiple steps during the development of the 4<sup>th</sup> PAAs .

## Figure Legends

### **Figure 1. The 4<sup>th</sup> PAA contains the highest proportion of SHF-derived ECs. A.**

Whole-mount IF and 3D-reconstruction of lineage label in *Mef2C-AHF-Cre* E10.5 embryo. **B.** Quantification of total EC numbers in each arch. **C – C'.** Quantification of the proportion of SHF-derived ECs in each PAA. Each dot in violin plots represents one arch, solid lines mark medians, dashed lines mark quartiles.

**Figure 2. Endothelial PAA progenitors in the second heart field.** Tamoxifen was injected at the specified times and embryos were dissected at E10.5. **A.** Highest labeling of PAA endothelium occurred when tamoxifen was injected at 5 AM in at E7.5 in *Isl1<sup>CreER</sup>* knock-in mice. **B.** Peak labeling occurred at 10 PM at E7.5 in *MEF2C-AHF-DreERT2* strain. Data from **B** is replotted at a different scale for E8.5 and E9.5 labeling experiments in **B1** and **B2**. **B1.** Labeling of the 4<sup>th</sup> and 6<sup>th</sup> PAAs is more efficient at E8.5 than the labeling of the 3<sup>rd</sup> PAAs. **B2.** The labeling of 4<sup>th</sup> and 6<sup>th</sup> PAAs continue when the labeling for the 3<sup>rd</sup> PAAs has stopped.

**Figure 3. The expression of integrin  $\alpha 5$  in the *Isl1* lineages does not impair the contribution of the SHF to the heart or pharyngeal arches.** E9.5 embryos 18-24 somites were analyzed. **A.** Quantification of the number of *Isl1*-lineage mesodermal cells posterior to the 2<sup>nd</sup> arch. **B.** Quantification of *Isl1*-lineage cells in the mesenchyme of posterior arches (3 – 6). **C.** Quantification of VEGFR2 pixels within GFP+ pixels. **D.** Quantification of *Isl1*-lineage cells in the entire heart and **E.** in the outflow tract (OFT) and the right ventricle (RV). Each dot mark one embryo in **A**, **C – D**, or one side in **B**. Controls *Itga5*<sup>flox/+</sup>; *Isl1*<sup>Cre/+</sup>, M-mutants *Itga5*<sup>flox/-</sup>; *Isl1*<sup>Cre/+</sup>

**Figure 4. Integrin  $\alpha 5$  expressed in the *Isl1* lineages regulates the accrual of ECs in the 4<sup>th</sup> pharyngeal arches.** **A.** Endothelial cell number is decreased in *Itga5*<sup>flox/-</sup>; *Isl1*<sup>Cre/+</sup> mutants relative to controls. **B.** The volume of the 4<sup>th</sup> pharyngeal mesenchyme was similar in mutants and controls. **C.** Endothelial population in the 4<sup>th</sup> arch of mutants has caught up with that of controls.

**Figure 5. Formation of the 4<sup>th</sup> PAA is delayed in *Fn1*<sup>flox/-</sup>; *Isl1*<sup>Cre</sup> and integrin  $\alpha 5$ <sup>flox/-</sup>; *Isl1*<sup>Cre</sup> mutants.** Control and mutant embryos dissected at different somite stages on the 10<sup>th</sup> day of development were stained to detect *Pecam1*. PAAs are numbered and somite stages are indicated. **A, D, G, J.** 3D reconstructions of whole-mount *Pecam1* staining (light blue). **B, E, H, K.** PAA endothelium in the 3<sup>rd</sup>, 4<sup>th</sup> and 6<sup>th</sup> arches shown in the row above was surface-rendered white, green and red, respectively. In addition, the plexus endothelium in the 4<sup>th</sup> arch was surface-rendered pink. **C, F, I, L.** Left side and ventral views of surface-rendered PAAs and the plexus. Development of the 4<sup>th</sup> PAAs was specifically affected in the mutants. PAAs appear oval because of slight squishing of embryos under the cover slip. Magnification is the same in all panels. Scale bar is 100  $\mu$ m. **M – N.** Analyses using combined data from *Fn1*<sup>flox/-</sup>; *Isl1*<sup>Cre/+</sup> and *Itga5*<sup>flox/-</sup>; *Isl1*<sup>Cre/+</sup> mutants and their littermate controls. **M** The rearrangement of the pharyngeal plexus into an artery in the 4<sup>th</sup> arch was defective in the mutants at all stages analyzed during the 10<sup>th</sup> day of embryonic development. **N.** Proliferation of endothelial cells within the two endothelial compartments in the 4<sup>th</sup> arches was similar in mutants and controls. In all violin plots, solid lines mark the median, and dashed lines mark the quartiles.

**Figure 6. Integrin  $\alpha 5$  and Fn1 regulate the remodeling of EC plexus during the formation of the 4<sup>th</sup> pharyngeal arch arteries. A – C.** Linear regression analyses indicate the absence of linear correlation between endothelial cell number or density and the size of the 4<sup>th</sup> PAA (expressed as the percentage of pharyngeal arch endothelial cells in the 4<sup>th</sup> PAA) in control embryos. **C.** Endothelial cell numbers from mutants with defective (open symbols) and unaffected 4<sup>th</sup> PAA (closed symbols) were plotted vs the size of the 4<sup>th</sup> PAAs. Regression analysis indicated low correlation between these properties. Circles: 32 – 33 somite embryos, rhombi: 34 – 35 somite embryos, triangles: 36 – 39 somite embryos. **D.** The rearrangement of the endothelial plexus into the 4<sup>th</sup> PAAs is defective in mutants relative to controls with the same number of endothelial cells in the arch. EC – endothelial cell(s).

**Figure 7. The expression of integrin  $\alpha 5$  in the Isl1 lineages regulates the differentiation of neural crest-derived cells into VSCMs at E11.5 A.** PAA diameter has recovered in size in the mutants by E11.5. **B.** Smooth muscle coverage of the left 4<sup>th</sup> and left 6<sup>th</sup> PAA was deficient in the mutants. **C.** Activation of Notch in the pharyngeal arch mesenchyme is not altered in the mutants.

Green fluorescent protein (GFP, green) marks the Isl1 lineages; Notch intracellular domain (NICD, orange) is used as the readout of active Notch signaling; alpha smooth muscle actin (ASMA, blue) marks smooth muscle cells. PAAs are numbered. The magnification is the same in all panels. Scale bar (shown in the bottom right panel) is 50  $\mu$ m.

**Supplemental Figure 1. The differentiation of VEGFR2+ endothelial cells into Pecam1+ endothelial cells is not affected by the deletion of integrin  $\alpha 5$  in the Isl1 lineages.** Whole-mount staining, confocal imaging and 3D reconstruction through the pharyngeal regions of a control and a mutant with defective formation of the 4<sup>th</sup> PAA. All VEGFR2+ cells are Pecam1+. Scale bars are 50  $\mu$ m.

**Supplemental Figure 2. Delayed formation of the 4<sup>th</sup> PAAs in mutants lacking integrin  $\alpha 5$  or Fn1 in the Isl1 lineages. A.** PAAs are either not evident or thin in the mutants. Whole-mount immunofluorescence and 3D reconstruction of the pharyngeal

vasculature at 33- and 36- somite stages. Endothelial cells in the 4<sup>th</sup> arches are highlighted in yellow. PAAs are numbered, arrows point to the 4<sup>th</sup> PAAs. All scale bars are 50  $\mu$ m. **B – C.** Quantification of total endothelial cell numbers in the 4<sup>th</sup> arches of controls and mutants show similar phenotypes between integrin  $\alpha 5^{flox/-}$ ;  $Isl1^{Cre/+}$  and  $Fn1^{flox/-}$ ;  $Isl1^{Cre/+}$  embryos. Note the recovery of endothelial cell numbers at 36 – 40-somite stage. **D – E.** Combined data comparing endothelial populations of controls and integrin  $\alpha 5^{flox/-}$ ;  $Isl1^{Cre/+}$  and  $Fn1^{flox/-}$ ;  $Isl1^{Cre/+}$  mutant embryos at 33 – 34-somite stages. **D.** Endothelial cell numbers are decreased in the mutants relative to controls. **E.** The proportion of endothelial cells in the PAA is decreased in the mutants relative to controls. Note, 7 of 16 mutants did not have PAAs (0% endothelial cells in the 4<sup>th</sup> PAA).

**Supplemental Figure 3. Step-wise changes in the configuration of the 4<sup>th</sup> arch endothelium on the 10<sup>th</sup> day of mouse embryonic development.** Embryos were stained using antibody to Pecam1. Endothelial cells in the 4<sup>th</sup> pharyngeal arch were surface-rendered yellow using IMARIS. First row, 30-somite stage. Endothelium in the 4<sup>th</sup> arch is in the form of a plexus of small blood vessels. Second row 33-somite embryo. A small PAA is seen forming. Red stars mark spaces among the interconnected plexus vessels and the small PAA. Third row, 36-somite stage. A large PAA is seen with connecting plexus vessels. Spaces (e.g. marked by the red stars) are still seen. Fourth row – 36 – 40 – somite stage. A large PAA is present in the 4<sup>th</sup> arch by the evening of the 10<sup>th</sup> day. DA – dorsal aorta. PAAs are numbers. All scale bars are 50  $\mu$ m.

**Supplemental Figure 4.** Cell death, as assayed by the presence of cleaved caspase 3 or the TUNEL signals, was similar in controls and mutants. **A, C.** Controls. **B, D.** Mutants. All scale bars are 100  $\mu$ m.

**Supplemental Figure 5. PAA formation is not affected when integrin  $\alpha 5b1$  is ablated using Sox17<sup>2A-iCre</sup> knock-in strain.** Whole-mount pictures were taken following India Ink injections into the hearts of controls and mutants isolated at E10.5. Magnification is the same in all panels.



## Acknowledgements

We thank Richard Hynes, Chenleng Cai, Sylvia Evans, Benoit Bruneau, Heicko Lickert, and Hongkui Zeng for the gift of mouse strains.

## Sources of Funding

This work was supported by the funding from the National Heart, Lung, and Blood Institute of the NIH R01 HL103920, R01 HL134935, and R21 OD025323-01 to SA, and pre-doctoral fellowship F31HL150949 to AJR.

## Disclosures

None

## References

- Abrial, M., Paffett-Lugassy, N., Jeffrey, S., Jordan, D., O'Loughlin, E., Frederick, C.J., 3rd, Burns, C.G., Burns, C.E., 2017. TGF-beta Signaling Is Necessary and Sufficient for Pharyngeal Arch Artery Angioblast Formation. *Cell Rep* 20, 973-983.
- Alfano, D., Altomonte, A., Cortes, C., Bilio, M., Kelly, R.G., Baldini, A., 2019. Tbx1 regulates extracellular matrix-cell interactions in the second heart field. *Human molecular genetics* 28, 2295-2308.
- Bockman, D.E., Redmond, M.E., Waldo, K., Davis, H., Kirby, M.L., 1987. Effect of neural crest ablation on development of the heart and arch arteries in the chick. *The American journal of anatomy* 180, 332-341.
- Bremer, J.L., 1912. The development of the aorta and aortic arches in rabbits. *American Journal of Anatomy* 13, 111-128.
- Cai, C.L., Liang, X., Shi, Y., Chu, P.H., Pfaff, S.L., Chen, J., Evans, S., 2003. Isl1 identifies a cardiac progenitor population that proliferates prior to differentiation and contributes a majority of cells to the heart. *Dev Cell* 5, 877-889.
- Calmont, A., Ivins, S., Van Bueren, K.L., Papangelis, I., Kyriakopoulou, V., Andrews, W.D., Martin, J.F., Moon, A.M., Illingworth, E.A., Basson, M.A., Scambler, P.J., 2009. Tbx1 controls cardiac neural crest cell migration during arch artery development by regulating Gbx2 expression in the pharyngeal ectoderm. *Development* 136, 3173-3183.

Chen, D., Wang, X., Liang, D., Gordon, J., Mittal, A., Manley, N., Degenhardt, K., Astrof, S., 2015. Fibronectin signals through integrin  $\alpha 5 \beta 1$  to regulate cardiovascular development in a cell type-specific manner. *Dev Biol* 407, 195-210.

DeRuiter, M.C., Poelmann, R.E., Mentink, M.M., Vaniperen, L., Gittenberger-De Groot, A.C., 1993. Early formation of the vascular system in quail embryos. *Anat Rec* 235, 261-274.

Devine, W.P., Wythe, J.D., George, M., Koshiba-Takeuchi, K., Bruneau, B.G., 2014. Early patterning and specification of cardiac progenitors in gastrulating mesoderm. *eLife* 3.

Dodou, E., Verzi, M.P., Anderson, J.P., Xu, S.M., Black, B.L., 2004. Mef2c is a direct transcriptional target of ISL1 and GATA factors in the anterior heart field during mouse embryonic development. *Development* 131, 3931-3942.

Engert, S., Liao, W.P., Burtscher, I., Lickert, H., 2009. Sox17-2A-iCre: a knock-in mouse line expressing Cre recombinase in endoderm and vascular endothelial cells. *Genesis* 47, 603-610.

Engleka, K.A., Manderfield, L.J., Brust, R.D., Li, L., Cohen, A., Dymecki, S.M., Epstein, J.A., 2012. Islet1 derivatives in the heart are of both neural crest and second heart field origin. *Circ Res* 110, 922-926.

Francou, A., Saint-Michel, E., Mesbah, K., Kelly, R.G., 2014. TBX1 regulates epithelial polarity and dynamic basal filopodia in the second heart field. *Development* 141, 4320-4331.

Gitler, A.D., Lu, M.M., Epstein, J.A., 2004. PlexinD1 and semaphorin signaling are required in endothelial cells for cardiovascular development. *Dev Cell* 7, 107-116.

Gittenberger-de Groot, A.C., DeRuiter, M.C., Bergwerff, M., Poelmann, R.E., 1999. Smooth muscle cell origin and its relation to heterogeneity in development and disease. *Arterioscler Thromb Vasc Biol* 19, 1589-1594.

Guner-Ataman, B., Gonzalez-Rosa, J.M., Shah, H.N., Butty, V.L., Jeffrey, S., Abrial, M., Boyer, L.A., Burns, C.G., Burns, C.E., 2018. Failed Progenitor Specification Underlies the Cardiopharyngeal Phenotypes in a Zebrafish Model of 22q11.2 Deletion Syndrome. *Cell Rep* 24, 1342-1354 e1345.

Guner-Ataman, B., Paffett-Lugassy, N., Adams, M.S., Nevis, K.R., Jahangiri, L., Obregon, P., Kikuchi, K., Poss, K.D., Burns, C.E., Burns, C.G., 2013. Zebrafish second

heart field development relies on progenitor specification in anterior lateral plate mesoderm and nkx2.5 function. *Development* 140, 1353-1363.

Hellstrom, M., Gerhardt, H., Kalen, M., Li, X., Eriksson, U., Wolburg, H., Betsholtz, C., 2001. Lack of pericytes leads to endothelial hyperplasia and abnormal vascular morphogenesis. *J Cell Biol* 153, 543-553.

High, F.A., Jain, R., Stoller, J.Z., Antonucci, N.B., Lu, M.M., Loomes, K.M., Kaestner, K.H., Pear, W.S., Epstein, J.A., 2009. Murine Jagged1/Notch signaling in the second heart field orchestrates Fgf8 expression and tissue-tissue interactions during outflow tract development. *J Clin Invest* 119, 1986-1996.

High, F.A., Lu, M.M., Pear, W.S., Loomes, K.M., Kaestner, K.H., Epstein, J.A., 2008. Endothelial expression of the Notch ligand Jagged1 is required for vascular smooth muscle development. *Proceedings of the National Academy of Sciences* %R 10.1073/pnas.0709663105 105, 1955-1959.

High, F.A., Zhang, M., Proweller, A., Tu, L., Parmacek, M.S., Pear, W.S., Epstein, J.A., 2007. An essential role for Notch in neural crest during cardiovascular development and smooth muscle differentiation. *J Clin Invest* 117, 353-363.

Holowiecki, A., Linstrum, K., Ravisankar, P., Chetal, K., Salomonis, N., Waxman, J.S., 2020. Pbx4 limits heart size and fosters arch artery formation through partitioning second heart field progenitors and restricting proliferation. *Development*.

Hutson, M.R., Kirby, M.L., 2007. Model systems for the study of heart development and disease. Cardiac neural crest and conotruncal malformations. *Semin Cell Dev Biol* 18, 101-110.

Hutson, M.R., Sackey, F.N., Lunney, K., Kirby, M.L., 2009. Blocking hedgehog signaling after ablation of the dorsal neural tube allows regeneration of the cardiac neural crest and rescue of outflow tract septation. *Dev Biol* 335, 367-373.

Jia, G., Preussner, J., Chen, X., Guenther, S., Yuan, X., Yekelchik, M., Kuenne, C., Looso, M., Zhou, Y., Teichmann, S., Braun, T., 2018. Single cell RNA-seq and ATAC-seq analysis of cardiac progenitor cell transition states and lineage settlement. *Nat Commun* 9, 4877.

Keyte, A., Hutson, M.R., 2012. The neural crest in cardiac congenital anomalies. *Differentiation; research in biological diversity* 84, 25-40.

Kirby, M.L., 2007. *Cardiac Development*. Oxford University Press, New York.

Li, P., Pashmforoush, M., Sucov, H.M., 2012. Mesodermal retinoic acid signaling regulates endothelial cell coalescence in caudal pharyngeal arch artery vasculogenesis. *Dev Biol* 361, 116-124.

Liang, D., Wang, X., Mittal, A., Dhiman, S., Hou, S.Y., Degenhardt, K., Astrof, S., 2014. Mesodermal expression of integrin alpha5beta1 regulates neural crest development and cardiovascular morphogenesis. *Dev Biol* 395, 232–244.

Macatee, T.L., Hammond, B.P., Arenkiel, B.R., Francis, L., Frank, D.U., Moon, A.M., 2003. Ablation of specific expression domains reveals discrete functions of ectoderm- and endoderm-derived FGF8 during cardiovascular and pharyngeal development. *Development* 130, 6361-6374.

Madisen, L., Garner, A.R., Shimaoka, D., Chuong, A.S., Klapoetke, N.C., Li, L., van der Bourg, A., Niino, Y., Egolf, L., Monetti, C., Gu, H., Mills, M., Cheng, A., Tasic, B., Nguyen, T.N., Sunkin, S.M., Benucci, A., Nagy, A., Miyawaki, A., Helmchen, F., Empson, R.M., Knopfel, T., Boyden, E.S., Reid, R.C., Carandini, M., Zeng, H., 2015. Transgenic mice for intersectional targeting of neural sensors and effectors with high specificity and performance. *Neuron* 85, 942-958.

Manderfield, L.J., Aghajanian, H., Engleka, K.A., Lim, L.Y., Lui, F., Jain, R., Li, L., Olson, E.N., Epstein, J.A., 2015. Hippo signaling is required for Notch-dependent smooth muscle differentiation of neural crest. *Development*.

Manderfield, L.J., High, F.A., Engleka, K.A., Liu, F., Li, L., Rentschler, S., Epstein, J.A., 2012. Notch activation of Jagged1 contributes to the assembly of the arterial wall. *Circulation* 125, 314-323.

Merscher, S., Funke, B., Epstein, J.A., Heyer, J., Puech, A., Lu, M.M., Xavier, R.J., Demay, M.B., Russell, R.G., Factor, S., Tokooya, K., Jore, B.S., Lopez, M., Pandita, R.K., Lia, M., Carrion, D., Xu, H., Schorle, H., Kobler, J.B., Scambler, P., Wynshaw-Boris, A., Skoultschi, A.I., Morrow, B.E., Kucherlapati, R., 2001. TBX1 is responsible for cardiovascular defects in velo-cardio-facial/DiGeorge syndrome. *Cell* 104, 619-629.

Momma, K., 2010. Cardiovascular anomalies associated with chromosome 22q11.2 deletion syndrome. *Am J Cardiol* 105, 1617-1624.

Moon, A., 2008. Mouse models of congenital cardiovascular disease. *Curr Top Dev Biol* 84, 171-248.

Muzumdar, M.D., Tasic, B., Miyamichi, K., Li, L., Luo, L., 2007. A global double-fluorescent Cre reporter mouse. *Genesis* 45, 593-605.

Nagelberg, D., Wang, J., Su, R., Torres-Vazquez, J., Targoff, K.L., Poss, K.D., Knaut, H., 2015. Origin, Specification, and Plasticity of the Great Vessels of the Heart. *Curr Biol* 25, 2099-2110.

Paffett-Lugassy, N., Singh, R., Nevis, K.R., Guner-Ataman, B., O'Loughlin, E., Jahangiri, L., Harvey, R.P., Burns, C.G., Burns, C.E., 2013. Heart field origin of great vessel precursors relies on nkx2.5-mediated vasculogenesis. *Nat Cell Biol* 15, 1362-1369.

Phillips, H.M., Stothard, C.A., Shaikh Qureshi, W.M., Kousa, A.I., Briones-Leon, J.A., Khasawneh, R.R., O'Loughlin, C., Sanders, R., Mazzotta, S., Dodds, R., Seidel, K., Bates, T., Nakatomi, M., Cockell, S.J., Schneider, J.E., Mohun, T.J., Maehr, R., Kist, R., Peters, H., Bamforth, S.D., 2019. Pax9 is required for cardiovascular development and interacts with Tbx1 in the pharyngeal endoderm to control 4th pharyngeal arch artery morphogenesis. *Development* 146.

Psillas, G., Kekes, G., Constantinidis, J., Triaridis, S., Vital, V., 2007. Subclavian steal syndrome: neurotological manifestations. *Acta Otorhinolaryngol Ital* 27, 33-37.

Ramirez, A., Astrof, S., 2020. Visualization and Analysis of Pharyngeal Arch Arteries using Whole-mount Immunohistochemistry and 3D Reconstruction. *J. Vis. Exp.* 157, e60797.

Rosenquist, T.H., Kirby, M.L., van Mierop, L.H., 1989. Solitary aortic arch artery. A result of surgical ablation of cardiac neural crest and nodose placode in the avian embryo. *Circulation* 80, 1469-1475.

Scambler, P.J., 2000. The 22q11 deletion syndromes. *Human molecular genetics* 9, 2421-2426.

Stoller, J.Z., Epstein, J.A., 2005. Cardiac neural crest. *Semin Cell Dev Biol* 16, 704-715.

Sun, Y., Liang, X., Najafi, N., Cass, M., Lin, L., Cai, C.L., Chen, J., Evans, S.M., 2007. Islet 1 is expressed in distinct cardiovascular lineages, including pacemaker and coronary vascular cells. *Dev Biol* 304, 286-296.

van der Flier, A., Badu-Nkansah, K., Whittaker, C.A., Crowley, D., Bronson, R.T., Lacy-Hulbert, A., Hynes, R.O., 2010. Endothelial alpha5 and alphav integrins cooperate in remodeling of the vasculature during development. *Development* 137, 2439-2449.

Verzi, M.P., McCulley, D.J., De Val, S., Dodou, E., Black, B.L., 2005. The right ventricle, outflow tract, and ventricular septum comprise a restricted expression domain within the secondary/anterior heart field. *Dev Biol* 287, 134-145.

Wagner, S., Chiosea, S., Nickerson, J.A., 2003. The spatial targeting and nuclear matrix binding domains of SRm160. *Proc Natl Acad Sci U S A* 100, 3269-3274.

Wang, X., Astrof, S., 2016. Neural crest cell-autonomous roles of fibronectin in cardiovascular development. *Development* 143, 88-100.

Wang, X., Chen, D., Chen, K., Jubran, A., Ramirez, A., Astrof, S., 2017. Endothelium in the pharyngeal arches 3, 4 and 6 is derived from the second heart field. *Dev Biol* 421, 108-117.

Yang, J.T., Hynes, R.O., 1996. Fibronectin receptor functions in embryonic cells deficient in alpha 5 beta 1 integrin can be replaced by alpha V integrins. *Mol Biol Cell* 7, 1737-1748.

Figure 1

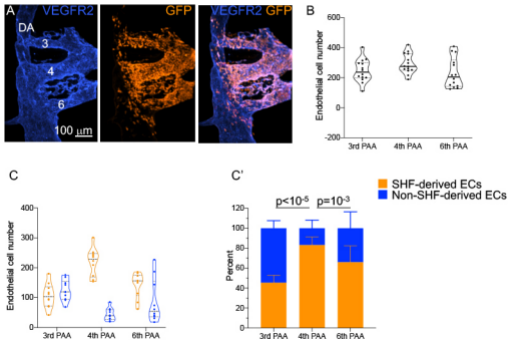
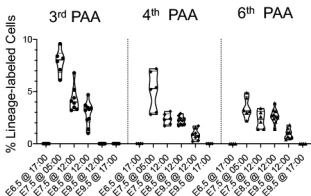


Figure 2

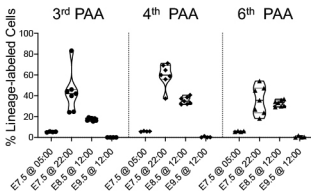
A

Isl1<sup>CreER</sup>

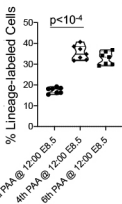


B

Mef2C-AHF-DreERT2



B1



B2

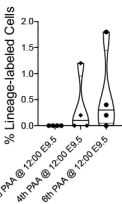


Figure 3

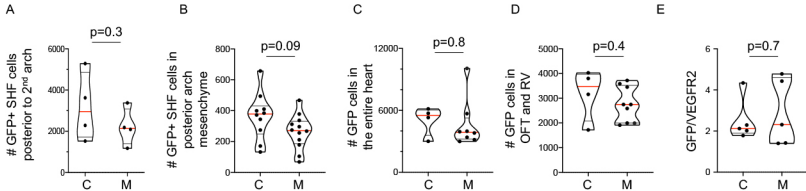


Figure 4

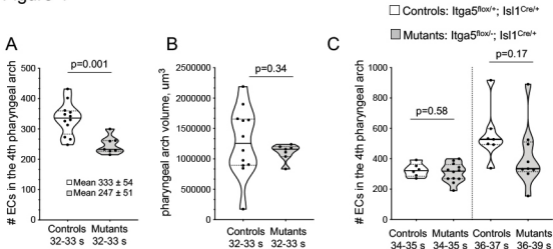
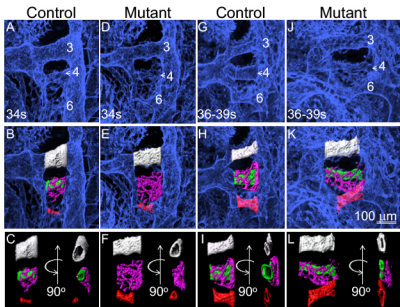
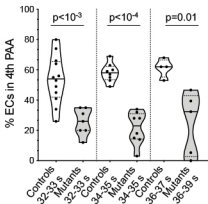


Figure 5



M



N

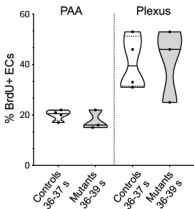
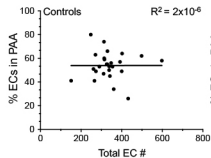
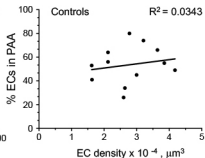


Figure 6

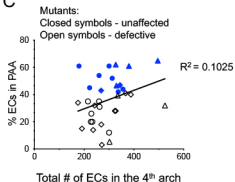
A



B



C



D

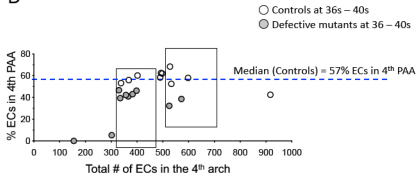
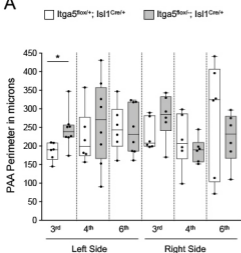
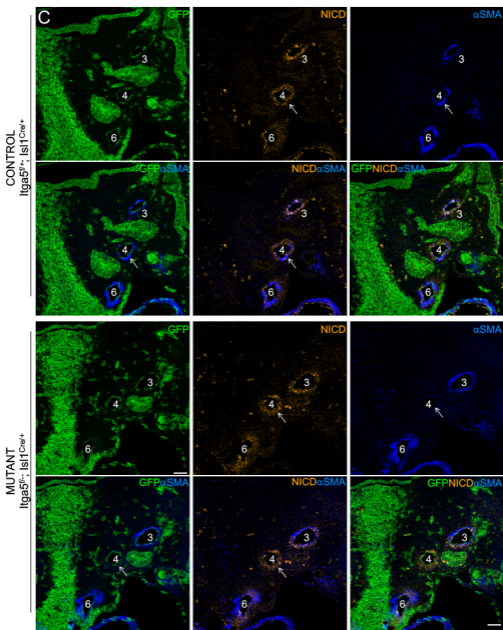
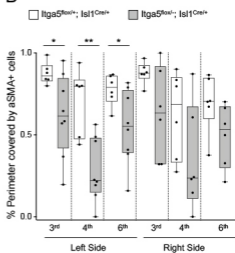


Figure 7

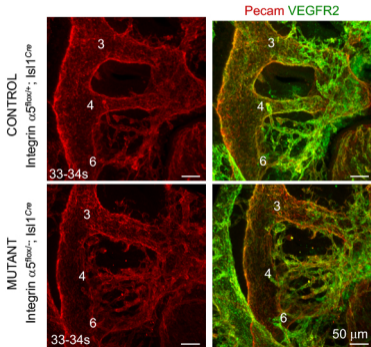
A



B

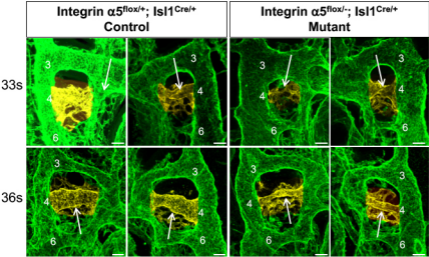


# Supplemental Figure 1



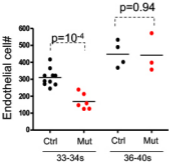
Supplemental Figure 2

A



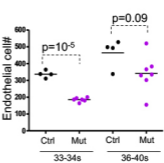
B

Ctrl:  $Fn1^{fl/-}; Isl1^{+/+}$  or  $Fn1^{fl/+}; Isl1^{Cre/+}$   
Mut:  $Fn1^{fl/-}; Isl1^{Cre/+}$

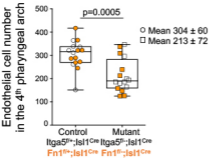


C

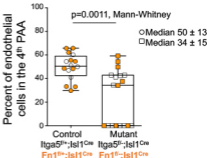
Ctrl:  $Itga5^{fl/-}; Isl1^{+/+}$  or  $Itga5^{fl/+}; Isl1^{Cre/+}$   
Mut:  $Itga5^{fl/-}; Isl1^{Cre/+}$



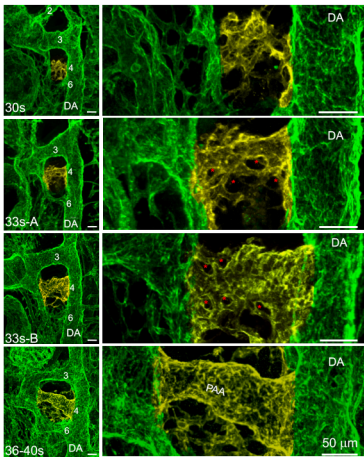
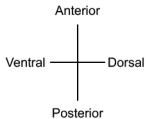
D



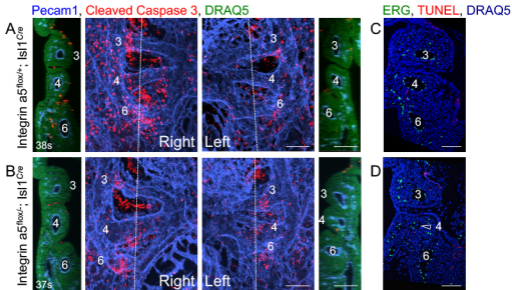
E



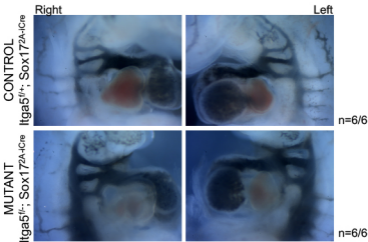
# Supplemental Figure 3



# Supplemental Figure 4



# Supplemental Figure 5



Supplemental Table 1. Itga5<sup>fl</sup> x Itga5<sup>+/-</sup>; Mef2C-AHF-Cre

Genotype	# Observed at Weaning
Itga5 <sup>fl/-</sup> ; Mef2C-AHF-Cre+	14
Itga5 <sup>fl/-</sup>	12
Itga5 <sup>fl/+</sup> ; Mef2C-AHF-Cre+	18
Itga5 <sup>fl/+</sup>	19
Total	63

Supplemental Table 2. Fn1<sup>fl</sup> x Fn1<sup>+/-</sup>; Mef2C-AHF-Cre

Genotype	# Observed at Weaning
Fn1 <sup>fl/-</sup> ; Mef2C-AHF-Cre+	23
Fn1 <sup>fl/-</sup>	15
Fn1 <sup>fl/+</sup> ; Mef2C-AHF-Cre+	17
Fn1 <sup>fl/+</sup>	19
Total	74